PFC/JA-89-4 Rev.

Neoclassical Analysis of Impurity Transport Following Transition to Improved Particle Confinement

Kevin W. Wenzel and Dieter J. Sigmar

October 1989

Submitted for publication in: *Nuclear Fusion, Letters*

Plasma Fusion Center

Massachusetts Institute of Technology

Cambridge, MA 02139

Neoclassical Analysis of Impurity Transport Following Transition to Improved Particle Confinement

K. W. Wenzel and D. J. Sigmar

MIT Plasma Fusion Center, Cambridge MA 02139

Abstract

Strongly peaked impurity density profiles have been observed in Alcator C after frozen hydrogen pellet injection. More recent experiments in ASDEX, PBX, TEXT, JET, and TFTR have exhibited similar impurity accumulation during regimes of improved confinement. In this context, we present calculations of the neoclassically predicted equilibrium profiles of the intrinsic impurities in Alcator C. These theoretical calculations were performed for comparison with the experimentally determined peaked profiles observed after pellet fueling. Profiles of the main impurities in Alcator, carbon (C) and molybdenum (Mo), were measured using soft x-ray diagnostics. C exists in the plateau collisionality regime, and its transport is dominated by collisions with the hydrogen background ions and temperature gradient effects. Mo is in the Pfirsch-Schlüter regime, and it is driven mostly by collisions with C inside $r/a \simeq 0.25$ and temperature gradients outside this radius. The rigorous multi-ion, mixed regime calculation necessary for the Mo transport is shown here. The predicted C profile is in excellent agreement with observation, and the profile predicted for Mo (which is not as close to equilibrium as C) is in fair agreement with observation.

1. Introduction

It is well known that transport processes in tokamaks have generally been measured to be anomalous. However, those discharges in the Alcator C tokamak with frozen fuel pellets injected into the plasma showed enhanced energy confinement [1] and strongly peaked, nearly neo-classical impurity density profiles [2]. More recent experiments on ASDEX [3-5], TEXT [6,7], JET [8] and TFTR [9] have also demonstrated impurity peaking on axis following the injection of frozen hydrogen pellets or the transition to other improved confinement regimes. Similarly, Z-dependent impurity accumulation, in general agreement with estimates of neoclassical transport, has been measured during neutral-beam-heated H mode discharges in PBX [10,11]. Furthermore, heavy impurity peaking in improved confinement modes in ASDEX has been accurately modelled using a neoclassical model [4], and light impurity peaking in high density discharges can also be explained by neoclassical models [5]. In this light, we outline the calculations of the predicted equilibrium impurity profiles for Alcator C using the neoclassical theory given by Hirshman and Sigmar [12], which has also been used by TFR [13] and ASDEX [4].

The transport of ions in the source-free central region of a tokamak plasma can be described theoretically by the simple expression of particle conservation

$$\frac{\partial n}{\partial t} + \nabla \cdot \mathbf{\Gamma} = 0, \tag{1}$$

where $\mathbf{\Gamma}$ is the flux of ions across the magnetic flux surfaces and n is the particle density. For the case of one impurity, the neoclassical impurity fluxes from Ref. [12] in various collisionality regimes have been rewritten in the simpler form [13] (with the correct temperature gradient terms added)

$$\Gamma_I^{CL} = \frac{\nu_{DI}\rho_D^2}{2Z_I T}\left[\frac{\partial P_D}{\partial r} - \frac{n_D}{Z_I n_I}\frac{\partial P_I}{\partial r} - 1.5 n_D \frac{\partial T}{\partial r}\right] \tag{2}$$

$$\Gamma_I^{P} = 1.25\frac{q}{R}\sqrt{m_I}\frac{T^{3/2}c^2 n_I}{B_T^2 Z_I e^2 n_D}\left[\frac{\partial n_D}{\partial r} - \frac{n_D}{Z_I n_I}\frac{\partial n_I}{\partial r} + \frac{1.5 n_D}{T}\frac{\partial T}{\partial r}\right] \tag{3}$$

$$\Gamma_I^{PS} = \frac{\nu_{DI}\rho_D^2}{2Z_I T}\left[2q^2\left(\frac{\partial P_D}{\partial r} - \frac{n_D}{Z_I n_I}\frac{\partial P_I}{\partial r}\right) - 3q^2 n_D \frac{\partial T}{\partial r}\right]. \quad (4)$$

In these expressions, Γ^{CL} is the classical contribution to the particle flux, Γ^P is the plateau flux, dominant for $\epsilon^{3/2} < \epsilon^{3/2}\nu_* < 1$, and Γ^{PS} is the Pfirsch-Schlüter contribution, dominant for $\epsilon^{3/2}\nu_* > 1$. The "collisionality" ν_* is defined as $\nu Rq/v_T\epsilon^{3/2}$, where for deuterium,

$$\nu_D \equiv \frac{16\sqrt{\pi}e^4 \ln\Lambda}{3m_D^2 v_{TD}^3}\left[\frac{n_D}{\sqrt{2}} + n_C Z_C^2 + n_{Mo}Z_{Mo}^2\right], \quad (5)$$

for carbon

$$\nu_C \equiv \frac{16\sqrt{\pi}e^4 Z_C^2 \ln\Lambda}{3m_C}\left[\frac{n_D}{m_D v_{TD}^3} + \frac{n_C Z_C^2}{\sqrt{2}m_C v_{TC}^3} + \frac{n_{Mo}Z_{Mo}^2}{m_C v_{TC}^3}\right], \quad (6)$$

and for molybdenum,

$$\nu_{Mo} \equiv \frac{16\sqrt{\pi}e^4 Z_{Mo}^2 \ln\Lambda}{3m_{Mo}}\left[\frac{n_D}{m_D v_{TD}^3} + \frac{n_C Z_C^2}{m_C v_{TC}^3} + \frac{n_{Mo}Z_{Mo}^2}{\sqrt{2}m_{Mo} v_{TMo}^3}\right]. \quad (7)$$

Here we used $\nu_{ab} = \tau_{ab}^{-1}$ from Eq. (A.30), if $m_a < m_b$. For $m_a = m_b$, $\nu_{aa} = (2^{-1/2})\nu_{ab}$. For $m_a > m_b$, following Trubnikov [14], $\nu_{ab} = \nu_{ba}\frac{m_b n_b}{m_a n_a}$. The thermal velocity $v_T = \sqrt{2T/m}$. Note that Eqs. (2)-(4) have the "standard form" $\Gamma_I = -D_I \partial n_I/\partial r - V_I n_I$ used in experimental analysis, and we have introduced the subscripts D for deuterium and I for the impurity.

In Alcator C (R=0.64 m, a=0.165 m) the main intrinsic impurities were carbon (C) and molybdenum (Mo). In the particular deuterium gas discharge considered here the experimental conditions were (see Fig. 3 of Ref. [2]) $T_{Mo} \simeq T_C \simeq T_D \simeq T_e \simeq 1.6$ keV at $r = 0$, and $n_{Mo}(0) \simeq 2.3\times 10^9$ cm^{-3}, $n_C(0) \simeq 1.4\times 10^{13}$ cm^{-3}, $n_D(0) \simeq n_e(0) \simeq 5.6\times 10^{14}$ cm^{-3}. Thus, defining the impurity strength parameter $\alpha_j = n_j Z_j^2/n_D$ ($\alpha_{Mo} = 3\times 10^{-3}$, $\alpha_C = 0.9$), we recall that if $\alpha_j >> \sqrt{m_e/m_D}$ the main ion collision friction $R_D = R_{De} + R_{Dj}$ is dominated by R_{Dj}, the ion impurity friction, rather than R_{De}, the ion-electron friction (cf. Appendix B). Thus C is a strong impurity and Mo is a trace impurity. All nine permutations of the central collision frequencies ν_{ab} where $a, b = D,\ C,\ Mo$ are given

in Table 1 along with the total collision frequencies and the ion thermal velocities. The relevant central values of the quantity $\epsilon^{3/2}\nu_*$ are $\epsilon^{3/2}\nu_*^C = 0.46$ and $\epsilon^{3/2}\nu_*^{Mo} = 40$. Hence we conclude that in the central region of interest C is clearly in the plateau regime and Mo is clearly in the Pfirsch-Schlüter regime. Radial profiles of the quantity $\epsilon^{3/2}\nu_*$ are shown in Fig. 1. Carbon lies in the plateau regime (between the dashed regime boundaries) from $r = 0$ to about $r = 10$ cm. Molybdenum, on the other hand, is in the Pfirsch-Schlüter regime across the entire plasma. In principle, this multi-ion situation does not present any calculational difficulties for C, since it is driven predominantly by the main deuterium ions. However, since the Mo flux is driven largely by the C, it is necessary to properly take into account the C and the existence of mixed regimes when calculating the Mo transport.

This letter is organized as follows. In Section 2 we briefly describe the calculation of the equilibrium profile for C. In Section 3, we describe the multi-ion, mixed regime calculation for the equilibrium profile of Mo. Conclusions are given in Section 4. In the Appendices, the required details of the neoclassical calculation are summarized for completeness.

2. Carbon

The equilibrium carbon density profile can be found simply by setting the radial flux equal to zero, using Equation (3) for the flux since C is in the plateau regime. Then

$$\frac{\partial n_D}{\partial r} - \frac{n_D}{Z_I n_I}\frac{\partial n_I}{\partial r} + \frac{1.5 n_D}{T}\frac{\partial T}{\partial r} = 0. \tag{8}$$

This has the solution

$$\frac{n_I(r)}{n_I(0)} = \left(\frac{n_D(r)}{n_D(0)}\right)^{Z_I}\left(\frac{T(r)}{T(0)}\right)^{1.5 Z_I}, \tag{9}$$

which is similar to the original result of Braginskii [15a] and Taylor [15b]. However Taylor assumed a flat temperature profile, in which case the C profile would not derive any additional peaking from temperature gradients. Note that if C were in the Pfirsch-Schlüter regime, the result for the C profile would be, from Equation (4), and recalling $p = nT$,

$$\frac{n_I(r)}{n_I(0)} = \left(\frac{n_D(r)}{n_D(0)}\right)^{Z_I}\left(\frac{T(r)}{T(0)}\right)^{-\frac{Z_I}{2}-1}. \tag{10}$$

In contrast to the result of Eq. (9), this would give *temperature screening* (*i.e.*, a negative temperature gradient causes a flatter C profile) instead of the *temperature peaking* implied by Eq. (9).

3. Molybdenum

The Mo impurity in Alcator C cannot be simply treated with the expressions (2)-(4) valid for one impurity frictioning on the main ion, because the Mo transport is dominated by effects from C [2], another impurity. In their review of neoclassical impurity transport, Hirshman and Sigmar include a rigorous expression including multi-ion effects (see Eq. 6.129 of Ref [12]). When this expression is applied to Mo, we obtain the flux

$$Z_{Mo}\Gamma_{Mo}^{PS} = -\left(\frac{2c^2Tq^2}{e^2B_o^2}\right)\times$$

$$\left[\frac{L_1}{Z_I}\frac{\partial \ln p_I}{\partial r} + \frac{L_2}{Z_I}\frac{\partial \ln p_I}{\partial r} + \frac{L_3}{Z_I}\frac{\partial \ln T}{\partial r} + \frac{L_{11}^{TD}}{Z_D}\frac{\partial \ln p_D}{\partial r} + \frac{L_{11}^{TT}}{Z_T}\frac{\partial \ln p_T}{\partial r} + \frac{L_{12}^{TD}}{Z_D}\frac{\partial \ln T}{\partial r}\right]. \quad (11)$$

The L coefficients are given in terms of the plasma parameters in Appendix A. The subscript I represents the dominant impurity (C), and the subscript T represents the trace impurity (Mo). All ion temperatures have been assumed to be the same.

Setting the radial trace impurity flux, Γ_{Mo}^{PS}, to zero gives

$$\frac{L_{11}^{TT}}{Z_T}\frac{\partial \ln n_T}{\partial r} + \left(\frac{L_1+L_2}{Z_I}\right)\frac{\partial \ln n_I}{\partial r} +$$

$$\left(\frac{L_1+L_2+L_3}{Z_I} + \frac{L_{11}^{TD}+L_{12}^{TD}}{Z_D} + \frac{L_{11}^{TT}}{Z_T}\right)\frac{\partial \ln T}{\partial r} + \left(\frac{L_{11}^{TD}}{Z_D}\right)\frac{\partial \ln n_D}{\partial r} = 0. \quad (12)$$

Now the Mo density equilibrium profile is easily obtained in terms of the equilibrium carbon density, the deuterium density and the temperature profiles

$$n_T(r) = n_T(0)\times \exp\left\{-\int_0^r \frac{Z_T}{L_{11}^{TT}}\left[\left(\frac{L_1+L_2}{Z_I}\right)\frac{\partial \ln n_I}{\partial r} + \right.\right.$$

$$\left.\left.\left(\frac{L_1+L_2+L_3}{Z_I} + \frac{L_{11}^{TD}+L_{12}^{TD}}{Z_D} + \frac{L_{11}^{TT}}{Z_T}\right)\frac{\partial \ln T}{\partial r} + \frac{L_{11}^{TD}}{Z_D}\frac{\partial \ln n_D}{\partial r}\right] dr\right\}. \quad (13)$$

Therefore, once the profile of the C density is known (from Eq. (9)) this can be easily integrated numerically to obtain the Mo density profile.

To put this in a simpler form similar to Eq. (9), we invoke the conditions predicted by Eq. (8) (and observed experimentally): $\partial \ln T/\partial r << \partial \ln n_C/\partial r$ and $\partial \ln n_D/\partial r << \partial \ln n_C/\partial r$. Then Eq. (12) becomes

$$\frac{\partial \ln n_T}{\partial r} = -\frac{Z_T}{Z_I}\left(\frac{L_1 + L_2}{L_{11}^{TT}}\right)\frac{\partial \ln n_I}{\partial r}, \tag{14}$$

which, using Eq. (9), has as an *approximate* solution

$$\frac{n_T(r)}{n_T(0)} = \left(\frac{n_I(r)}{n_I(0)}\right)^{\lambda(r)Z_T/Z_I} = \left(\frac{n_D(r)}{n_D(0)}\right)^{\lambda(r)Z_T}\left(\frac{T(r)}{T(0)}\right)^{1.5\lambda(r)Z_T}. \tag{15}$$

Note from Eq. (15) that the Mo peaking is driven by the C profile, which is itself peaked. In this expression $\lambda(r) = -(L_1 + L_2)/L_{11}^{TT}$, and is a slowly varying positive quantity of order one. The accurate value of $\lambda(r)$, calculated from the coefficients in Appendix A and the plasma parameters from Ref. [2], is shown in Fig. 2. It is important to note here that for Ref. [2] the more rigorous form of Eq. (13) including the deuterium density gradient and temperature gradient terms was used to predict the Mo profile for comparison to the experimental value.

4. Conclusions

The neoclassical theory for impurity transport predicts equilibrium density profiles more peaked than the electron density profile. In the case of mildly collisional carbon, in the plateau regime, the prediction is given by Eq. (9). For carbon this relation gives excellent agreement with the experimental observations [2]. For highly collisional molybdenum, in the trace impurity limit and in the Pfirsch-Schlüter regime, an exact form for the profiles is given by Eq. (13) and a simplified prediction is given by Eq. (15) with $\lambda(r)$ shown in Fig. 2. Note that the exponent in Eq. (15), $\lambda(r)Z_T/Z_I$ is smaller than one would estimate from the simpler cases considered in Ref. [15]. The predicted profile for Mo is not as close

to observation as is the carbon. However, the Mo is further from equilibrium than the carbon. If the time dependence were taken into account, the predicted profile would be broader, because the Mo would still be peaking. Moreover, since Mo is a trace impurity ($\alpha_{Mo} = 3 \cdot 10^{-3} < \sqrt{m_e/m_D}$) ambipolar friction between the Mo and the electrons can further broaden the predicted profiles (see Appendix B).

The present treatment does not constitute a full proof of neoclassical impurity transport since that would also require demonstrating that the experimental time scale to reach accumulation equilibrium agrees with time dependent neoclassical modelling. (This has not been shown here.) Furthermore it would require correct scaling with global plasma parameters. (Neoclassical scaling of the particle confinement time has been observed in the TJ-1 tokamak [16] but was not systematically tested in Ref. [2].) However, the observed agreement of the experimental carbon equilibrium profile and to a lesser degree, of molybdenum, with the detailed facets of equilibrium neoclassical theory appears to be highly suggestive of classical particle transport after pellet injection. At this time, a fully detailed calculation of a two-impurity-species, radially varying mixed collisionality regime plasma does not readily exist in the literature for use in time dependent modelling. (The full treatment is outlined in Appendix C.)

Acknowledgments

We gratefully acknowledge the strong motivating interest we received from Dr. Richard Petrasso, who provided the original observation of peaked impurity profiles in Alcator C, and thus the primary impetus for this work. This work was in part supported by U. S. Department of Energy Contract No. DE-AC02-78ET51013.

Appendix A. Neoclassical Coefficients

Coefficients for Equation (11) are summarized, from Ref. [12]. They are

$$L_1 = -\frac{m_I n_I}{\tau_{IT}}(d_0 + 0.236 d_3) - \frac{m_D n_D}{\tau_{DT}}[1 - C_1(\bar{Z}_{DI}, 0)], \tag{A.1}$$

$$L_2 = \frac{m_I n_I}{\tau_{IT}}(0.236 d_3), \tag{A.2}$$

$$L_3 = \frac{m_I n_I}{\tau_{IT}} d_3, \tag{A.3}$$

$$L_{11}^{TT} = \frac{m_I n_I}{\tau_{IT}} d_0 + \frac{m_D n_D}{\tau_{DT}}, \tag{A.4}$$

$$L_{11}^{TD} = \frac{m_D n_D}{\tau_{DT}} C_1(\bar{Z}_{DI}, 0), \tag{A.5}$$

$$L_{12}^{TD} = \frac{m_D n_D}{\tau_{DT}} C_2(\bar{Z}_{DI}, 0), \tag{A.6}$$

where the collision times τ_{ab} are defined below. The variables labeled d are

$$d_0 = -\left(\frac{m_T}{m_I}\right)^{1/2}\left[\hat{M}^{00} - \frac{\hat{M}^{01}\hat{M}^{10}}{\hat{M}^{11}}\right], \tag{A.7}$$

$$d_1 = 0.88\left(\frac{m_T}{m_I}\right)^{1/2}\left[\hat{N}^{01} - \frac{\hat{M}^{01}\hat{N}^{11}}{\hat{M}^{11}} - \frac{4}{15}\left(\hat{N}^{02} - \frac{\hat{M}^{01}\hat{N}^{12}}{\hat{M}^{11}}\right)\right], \tag{A.8}$$

$$d_2 = \frac{\hat{M}^{01}}{\hat{M}^{11}}, \tag{A.9}$$

$$d_3 = \frac{1}{0.885}\left[\left(\frac{Z_I^2}{Z_T^2}\right) d_2 - d_1\right], \tag{A.10}$$

Here, the coefficients C_1, C_2 as functions of two arbitrary variables α and β are

$$C_1(\alpha, \beta) = 1 - \frac{0.52\alpha}{0.59 + \alpha + 1.34\beta^2}, \tag{A.11}$$

$$C_2(\alpha, \beta) = 1.5 - \frac{0.29 + 1.20\alpha}{0.59 + \alpha + 1.34\beta^2}. \tag{A.12}$$

We also have defined

$$\bar{Z}_{DI} = \frac{n_I Z_I^2}{n_D}, \tag{A.13}$$

$$\beta = \omega_{TD}\tau_{TD}, \tag{A.14}$$

where ω_{TD} is the transit frequency of D,

$$\hat{M}^{ij} = M^{ij}_{TI} - \frac{M^{i2}_{TI} M^{2j}_{TI}}{M^{22}_{TI}}, \tag{A.15}$$

$$\hat{N}^{ij} = N^{ij}_{TI} - \frac{M^{i2}_{TI} N^{2j}_{TI}}{M^{22}_{TI}}. \tag{A.16}$$

For arbitrary species indices a and b one has

$$M^{00}_{ab} = -\left(1 + \frac{m_a}{m_b}\right)(1 + x^2_{ab})^{-3/2} = -N^{00}_{ab}, \tag{A.17}$$

$$M^{01}_{ab} = M^{10}_{ab} = -\frac{3}{2}\left(1 + \frac{m_a}{m_b}\right)(1 + x^2_{ab})^{-5/2} = -N^{10}_{ab}, \tag{A.18}$$

$$M^{11}_{ab} = -\left(\frac{13}{4} + 4x^2_{ab} + \frac{15}{2}x^4_{ab}\right)(1 + x^2_{ab})^{-5/2}, \tag{A.19}$$

$$N^{11}_{ab} = \frac{27}{4}\frac{T_a}{T_b}x^2_{ab}(1 + x^2_{ab})^{-5/2}, \tag{A.20}$$

$$M^{02}_{ab} = -\frac{15}{8}\left(1 + \frac{m_a}{m_b}\right)(1 + x^2_{ab})^{-7/2} = -x_{ba}N^{02}_{ba}, \tag{A.21}$$

$$M^{12}_{ab} = -\left(\frac{69}{16} + 6x^2_{ab} + \frac{63}{4}x^4_{ab}\right)(1 + x^2_{ab})^{-7/2}, \tag{A.22}$$

$$N^{12}_{ab} = \frac{225}{16}\frac{T_a}{T_b}x^4_{ab}(1 + x^2_{ab})^{-7/2}, \tag{A.23}$$

$$M^{22}_{ab} = -\frac{(443/64) + 17x^2_{ab} + (459/8)x^4_{ab} + 28x^6_{ab} + (175/8)x^8_{ab}}{(1 + x^2_{ab})^{9/2}}, \tag{A.24}$$

$$N^{22}_{ab} = \frac{2625}{64}\frac{T_a}{T_b}\frac{x^4_{ab}}{(1 + x^2_{ab})^{(9/2)}}, \tag{A.25}$$

$$x_{ab} = \frac{v_{Tb}}{v_{Ta}}, \tag{A.26}$$

where $v_{Ta} = \sqrt{2T/m_a}$. It is important to note that

$$M^{j0}_{ab} + N^{j0}_{ab} = 0, \tag{A.27}$$

$$M^{ij}_{ab} = M^{ji}_{ab}, \tag{A.28}$$

$$\frac{N^{ij}_{ab}}{T_a v_{Ta}} = \frac{N^{ji}_{ba}}{T_b v_{Tb}}, \tag{A.29}$$

and the collision time is taken from Braginskii to be

$$\tau_{ab} = \left(\frac{3\sqrt{\pi}}{4}\right)\frac{m^2_a v^3_{Ta}}{4\pi n_b e^2_a e^2_b \ln \Lambda} \qquad m_a < m_b\ . \tag{A.30}$$

Appendix B. Ambipolar Diffusion for a Two-Ion Species Plasma

Taking the toroidal momentum balance, the radial particle flux Γ_a follows from

$$0 = eZ_a\Gamma_a B_p + R_a; \quad R_a = \sum_{b\neq a} R_{ba} \ , \tag{B.1}$$

where the collisional friction is

$$R_{ab} = -m_a n_a \nu_{ab}(v_a - v_b) \ , \tag{B.2}$$

and [see Appendix A, Eq. (A.30)]

$$\nu_{ab} \sim Z_b^2 n_b/(\sqrt{m_a}T_a^{3/2}) \ , \tag{B.3}$$

and $v_a \sim v_{Ta}\rho_{pa}/r_n$. Here r_n is the radial scale length defined as $|n/(\partial n/\partial r)|^{-1}$, and ρ_{pa} is the poloidal gyroradius of species a, which can be e, D, C, or Mo in the case at hand. From Eqs. (B.1) and (B.2), and $R_{ab} = -R_{ba}$, follows the collisional transport ambipolarity condition

$$Z_{Mo}\Gamma_{Mo} = \Gamma_e - (\Gamma_D + Z_C\Gamma_C) \ . \tag{B.4}$$

Defining the impurity strength parameter,

$$\alpha_j = n_j Z_j^2/n_D; \quad j = C, \quad Mo \ , \tag{B.5}$$

and using the scaling expression (B.3) in (B.2), one finds in general $R_{eD}/R_{DI} \sim \sqrt{m_e/m_D}/\alpha_I$. Then $R_{eD}/R_{DC} \sim \sqrt{m_e/m_D}/\alpha_C \ll 1$, but $R_{eD}/R_{DMo} \sim \sqrt{m_e/m_D}/\alpha_{Mo} \gg 1$, $R_{DMo}/R_{DC} = \alpha_{Mo}/\alpha_C \ll 1$, and R_{CMo}/R_{DC} is entirely negligible (recalling $\alpha_C \sim 1$ and $\alpha_{Mo} \sim 3\times10^{-3}$). From (B.1), (B.2), (B.3), the deuterium flux scales as

$$\Gamma_D \sim R_{DC}\left(1 + \frac{\sqrt{m_e/m_D}}{\alpha_C} + \frac{\alpha_{Mo}}{\alpha_C}\right) \tag{B.6a}$$

and the carbon flux as

$$-Z_C\Gamma_C \sim R_{DC}\left(1 + \sqrt{\frac{m_e}{m_D}}\right) \ . \tag{B.6b}$$

Therefore, to zeroth order in $\sqrt{m_e/m_D}$

$$\Gamma_D^{(0)} + Z_C \Gamma_C^{(0)} = 0 \qquad (B.7a)$$

and for our case of $\alpha_{Mo}/\alpha_C < \sqrt{m_e/m_D}$

$$\Gamma_M^{(0)} = 0 \; . \qquad (B.7b)$$

This result is indeed borne out from Eq. (11) (or (4)) for molybdenum if one notices that $\nu_{IMo} \propto \alpha_{Mo}$ and is therefore of first order.

To obtain the first order flux $\Gamma_{Mo}^{(1)}$ the neoclassical electron flux must be retained which scales as

$$\Gamma_e \sim R_{DC} \frac{\sqrt{m_e/m_D}}{\alpha_C} (1 + \alpha_C + \alpha_{Mo}) \qquad (B.8)$$

and is thus of first order in $\sqrt{m_e/m_D}$. Thus, from (B.4)

$$Z_{Mo}\Gamma_{Mo}^{(1)} = \Gamma_e^{neo} + Z_{Mo}\Gamma_{Mo}(\text{from Eq. (11)}) \qquad (B.9)$$

where the last term derives from the Mo-D and Mo-C friction, including the thermal friction $\propto \frac{T'}{T}$. For Γ_e^{neo} one can take the usual electron banana regime expression

$$\Gamma_e^{neo} = -D_e^{BP} n_e \left(\frac{n_e'}{n_e}(1+\alpha) + \frac{n_i'}{n_i} + \frac{\alpha}{Z}\frac{n_z'}{n_z} + k_{BP}\frac{T'}{T} \right) + \Gamma_e(\text{Ware}) \; . \qquad (B.10)$$

We note that this is radially outward even when the ions have satisfied Eq. (8.7a). This outward flow will retard the Mo peaking. The Ware flux is inward. In Eq. (B.9), Γ_{Mo}(from Eq. (11)) is also inward. Thus, the overall rate of inward molybdenum transport will be affected by the detailed balance of the terms in Γ_e^{neo}. The exact equilibirum condition follows from setting the right hand side of Eq. (B.9) equal to zero, with Γ_e^{neo} from (B.10). This will lead to a dependence of the Mo equilibrium profile on the ratio of the electron diffusion coefficient D_e^{BP} in (B.10) and the diffusion coefficients contained in Eq. (11).

In all of the above, the turbulent driven fluxes $\tilde{\Gamma}_j$ (which for the typical low frequency turbulence in tokamaks have also been shown to be intrinsically ambipolar by themselves, i.e. $\sum_{j=e,D,I} e_j \tilde{\Gamma}_j = 0$) have been assumed to be decoupled from the collisionally driven fluxes of Eq. (B.1). This may be justified for the typically observed low saturation amplitudes $e\tilde{\phi}/T_e \gtrsim 10^{-2}$ in the plasma core. No turbulent theory exists giving the net fluctuation driven contribution including impurities to the right hand side of Eq. (B.9).

Appendix C. Outline of Calculation of Fluxes in Transitional Collisionality Regimes

It is shown in [12] that in general all three regime contributions to the flux $\Gamma_j \equiv \langle n_j \vec{v}_j \cdot \nabla\psi \rangle$, driven by the friction $\vec{R}_j$, must be kept. From toroidal momentum balance

$$e_j \Gamma_j = \langle R\vec{e}_\phi \cdot \left(R_{\|j} \frac{\vec{B}}{B} + \vec{R}_{\perp j} \right) \rangle =$$

$$= F \langle \frac{R_\| B}{B^2} \left(1 - \frac{B^2}{\langle B^2 \rangle} \right) \rangle + F \frac{\langle R_\| B \rangle}{\langle B^2 \rangle} + \langle R\vec{e}_\phi \cdot \vec{R}_{\perp j} \rangle$$

$$\equiv e_j \Gamma_j^{PS} + e_j \Gamma_j^{BP} + e_j \Gamma_j^{CL} \qquad (C.1)$$

where $F \equiv RB_\phi$. (Note that each piece is individually ambipolar which can be useful to know in mixed collisionality regimes.) From parallel momentum balance, to lowest order in ρ_{pol}/r_n,

$$O = -\langle \vec{B} \cdot \nabla \cdot \overleftrightarrow{\pi} \rangle + \langle B R_\| \rangle$$

which can be used to write

$$e_j \Gamma_j^{BP} = F \frac{\langle \vec{B} \cdot \nabla \cdot \overleftrightarrow{\pi}_j \rangle}{\langle B^2 \rangle} \ . \qquad (C.2)$$

It was shown (cf. [12]) that $\langle \vec{B} \cdot \nabla \cdot \overleftrightarrow{\pi}_j \rangle$ rises in the banana regime, peaks in the plateau and evanesces in the P.S. regime (where $\overleftrightarrow{\pi}_j$ is collisionally isotropized, but we note [17] that π_j can have contributions from unlike species collisions.)

In an impure plasma the P.S. flux (first term on right in (C.1)) is evidently driven by the poloidal variation of $\frac{R_{\|j}}{B}$ which can be shown [17] to scale with the parameter

$$\Delta \equiv (\rho_{pi}/r_n) Z^2 \frac{\nu_{ii}}{\omega_{ti}}$$

which is large in the P.S. regime and evanesces into the BP regime (where the long mean free path suppresses poloidal variations). The classical flux Γ^{CL} will also contribute near

the plasma center where $2q^2 \rightarrow 1$ (particularly if $q_o < 1$.) Thus, near the PS-BP transition, for each species j the flux becomes (cf. Eqs. (C.1), (C.2)).

$$\Gamma_j = -\sum_s D_{j,s} \frac{\partial n_j}{\partial r} - n_j V_{j,s}, \quad s = PS,\ BP,\ CL$$

i.e. s denotes the collisionality regime. $V_{j,s}$ is of the form

$$\frac{1}{e_k} \frac{n_k'}{n_k} + H_{j,s} \frac{T'}{T}, \quad \text{with } \mathrm{k} \neq \mathrm{j}\ .$$

$D_{j,s}$ and $H_{j,s}$ are functions of ϵ, ν_{*j} and $\alpha_j \equiv n_j Z_j^2 / n_D$, describing the transitions. (Not all transition details have been worked out yet in the literature.)

Clearly then, Eqs. (3), (4) or (11) are best valid in "clean" regimes away from transitions and Fig. 1 gives only a first guideline for the appropriate regimes. More accuracy is needed for time dependent impurity transport modelling than for the simple equilibrium profile determination attempted in this paper.

References

[1] M. Greenwald, D. Gwinn, S. Milora, J. Parker, R. Parker, *et. al.*, Phys. Rev. Lett. **53** (1984) 352; and M. Greenwald, M. Besen, F. Camacho, C. Fiore, M. Foord, *et. al.*, Plasma Physics and Controlled Nuclear Fusion Research 1986 (Proc. 11th Conf. Kyoto 1986) IAEA **1** (1987) 139.

[2] R. D. Petrasso, D. J. Sigmar, K. W. Wenzel, J. E. Hopf, M. Greenwald, J. L. Terry, and J. Parker, Phys Rev. Lett. **57** 707 (1986).

[3] M. Kaufmann, K. Büchl, G. Fussmann, O. Gehre, K. Grassie, *et. al.*, Nucl. Fusion **28** (1988) 827.

[4] G. Fussmann, J. Hofmann, G. Janeschitz, K. Krieger, E. R. Müller *et. al.*, J. Nucl. Mats. **162** 14 (1989).

[5] K. H. Steuer, H. Röhr, G. Fussmann, G. Janeschitz, A. Kallenbach *et. al.*, 16th European Conf. on Contr. Fusion and Plasma Phys., Venice, V13B, Part I, p. 191 (1989); see especially the conclusions.

[6] E. J. Synakowski, R. D. Bengtson, A. Ouroua, A. J. Wootton, S. K. Kim, Nucl. Fusion **29** 311 (1989).

[7] W. L. Rowan, R. V. Bravenec, J. C. Wiley, R. D. Bentgtson, R. D. Durst, *et. al.*, submitted to Nucl. Fusion (1988).

[8] P. Kupschus, Bull. Am. Phys. Soc. **33** (1988) 1977.

[9] R. A. Hulse, G. L. Schmidt, P. Efthimion, B. Grek, K. Hill, *et. al.*, Bull. Am. Phys. Soc. **33** (1988) 2095.

[10] K. Ida, R. J. Fonck, S. Sesnic, R. A. Hulse, B. LeBlanc, and S. F. Paul, Nucl. Fusion

29 231 (1989).

[11] K. Ida, R. J. Fonck, S. Sesnic, R. A. Hulse, and B. LeBlanc, Phys. Rev. Lett., **58** (1987) 116.

[12] S. P. Hirshman and D. J. Sigmar, Nucl. Fusion **21** (1981) 1079.

[13] TFR Group, Nucl. Fus. **22** 1173 (1982).

[14] B. A. Trubnikov, Reviews Plasma Phys., Vol. I, p. 190, Table 3, Consultants Bureau, NY 1965.

[15a] S. I. Braginskii, Sov. Phys.-JETP **6** (1958) 358.

[15b] J. B. Taylor, Phys. Fluids **4**, 1142 (1961).

[16] B. Zurro, C. Pardo, F. Mompeau, Plasma Phys. Contr. Fus. **30**, 1767 (1988).

[17] C. T. Hsu, D. J. Sigmar, submitted to Plasma Phys. Contr. Fus., 1989.

TABLE I lists the collision frequencies ν_{ab} (row a, column b) in the first three columns. The fourth column shows the total collision frequency for species a: $\nu_a^{total} = \sum_b \nu_{ab}$. The last column gives the thermal velocity for each species assuming all temperatures are equal to the central electron temperature of 1.6 keV.

Table I. Collision Frequencies (s^{-1}) and Thermal Velocities

	D	C	Mo	ν^{total}	v_T (cm/s)
D	4.34×10^3	6.18×10^3	2.54×10^1	1.05×10^4	3.91×10^7
C	3.68×10^5	6.43×10^4	3.73×10^2	1.55×10^5	1.60×10^7
Mo	1.15×10^5	2.84×10^5	2.33×10^3	4.02×10^5	5.65×10^6

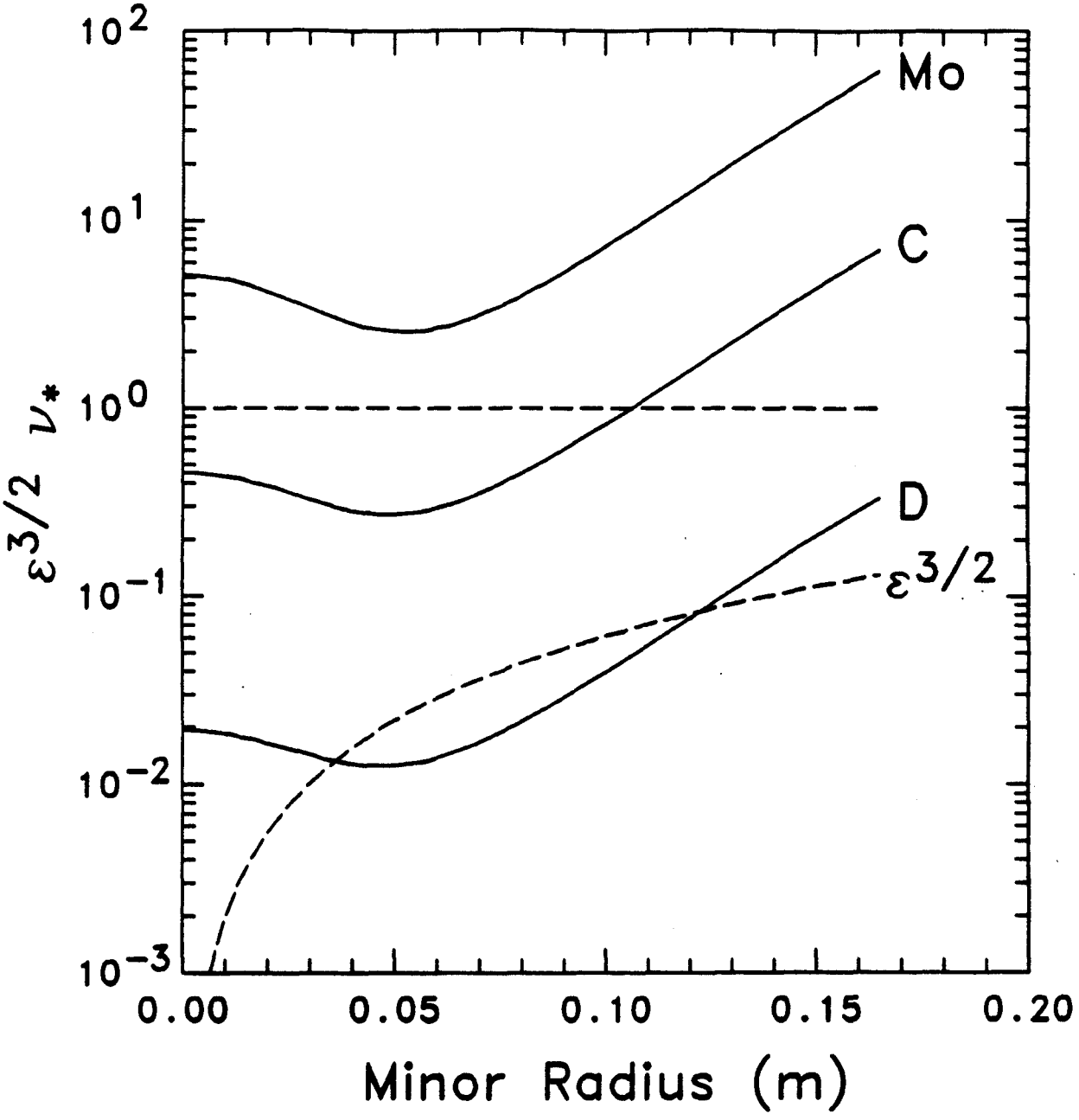

Fig. 1. The quantity $\epsilon^{3/2}\nu_*$ is shown for the three ion species in Alcator: deuterium (D), carbon (C), and molybdenum (Mo). The dashed lines represent transitions between different collisionality regimes. Mo is completely in the Pfirsch-Schlüter, and carbon is in the plateau inside about 10 cm.

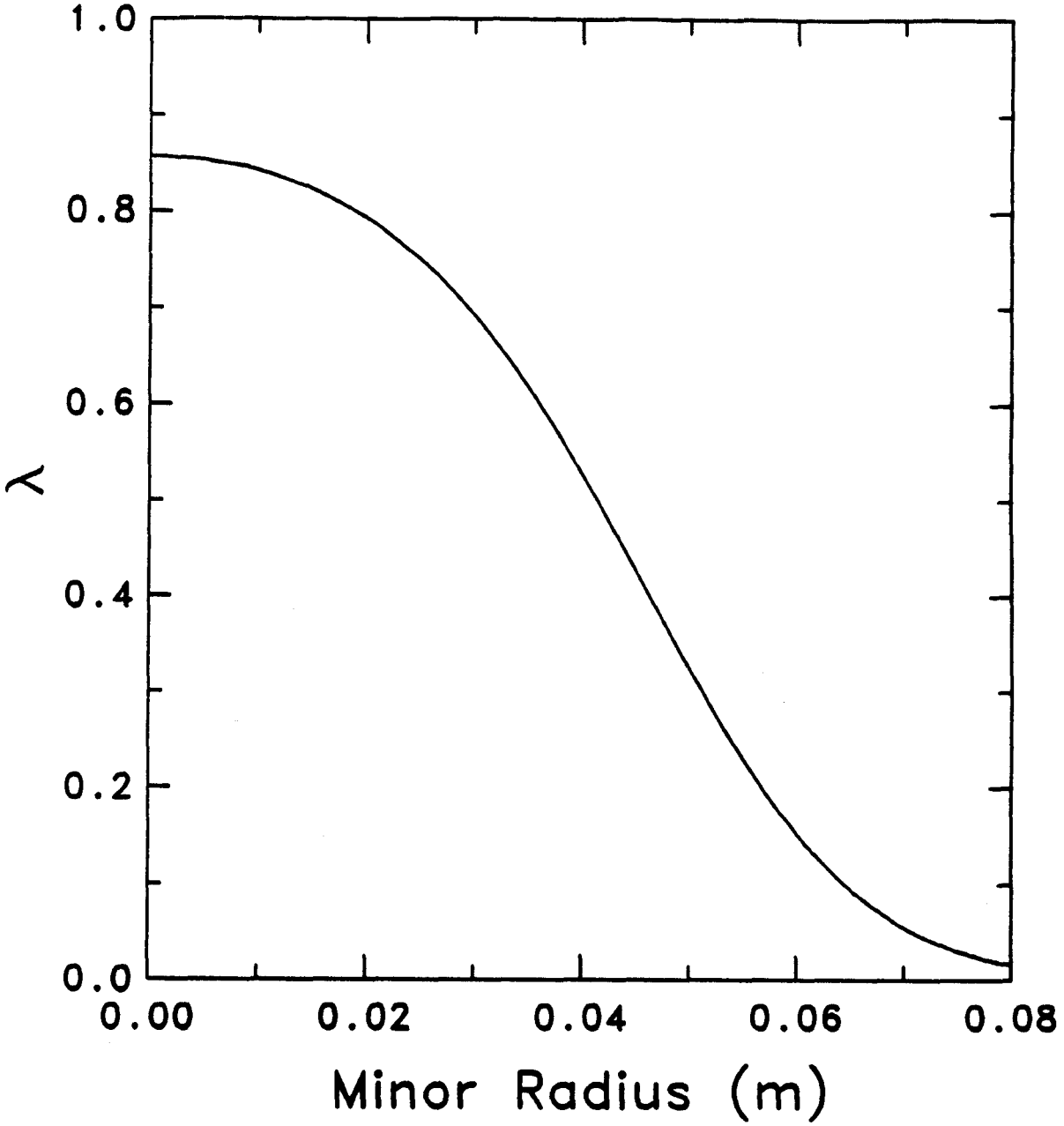

Fig. 2. The quantity $\lambda(r) = -(L_1 + L_2)/L_{11}^{TT}$, which occurs in Eq. (15) is shown for the parameters measured in a particular Alcator C discharge with deuterium gas, $B_T = 9.75T$ and $I_p = 520$ kA (see Ref. [2]).